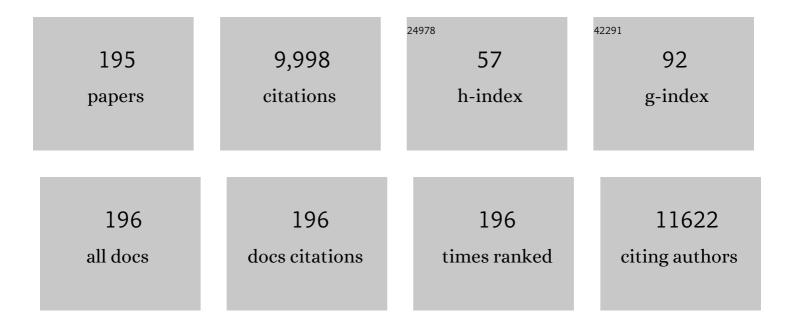
Bingqiang Cao

List of Publications by Year in descending order

Source: https://exaly.com/author-pdf/11870710/publications.pdf Version: 2024-02-01



RINCOLANC CAO

4

#	Article	IF	CITATIONS
1	A magnet-renewable electroanalysis strategy for hydrogen sulfide in aquaculture freshwater using magnetic silver metal-organic frameworks. Analytica Chimica Acta, 2022, 1195, 339450.	2.6	10
2	A bubble-templated approach to holey N/S-codoped carbon nanosheet aerogels with honeycomb-like structure for supercapacitors. Electrochimica Acta, 2022, 404, 139741.	2.6	13
3	Impact of Ferroelectric Domain Structure on Bulk Photovoltaic Effect of Epitaxial BiFe _{1â^²} <i>_x</i> Co <i>_x</i> O ₃ Films. Advanced Electronic Materials, 2022, 8, .	2.6	3
4	An ultrahigh 84.3% fill factor for efficient CH3NH3PbI3 P-i-N perovskite film solar cell. Solar Energy, 2022, 233, 271-277.	2.9	5
5	Cr2O3 interlayer at TiO2/perovskite interface propelling the efficiency improvement of perovskite solar cells. Surfaces and Interfaces, 2022, 29, 101761.	1.5	5
6	Stable CsPbX3 mixed halide alloyed epitaxial films prepared by pulsed laser deposition. Applied Physics Letters, 2022, 120, .	1.5	13
7	Enhancement of up-conversion luminescence through doping Ce3+ ions in YbxEr2â^'xTi2O7 thin films. Chemical Physics Letters, 2022, 795, 139498.	1.2	2
8	Bi3+ and Eu3+ co-doped CsPbCl3 perovskite quantum dots with efficient controllable blue emission via energy transfer. Journal of Luminescence, 2022, 247, 118901.	1.5	9
9	Dopant compensation in p-type doped MAPb _{1â^²} _{<i>x</i>} Cu _{<i>x</i>} I ₃ alloyed perovskite crystals. Applied Physics Letters, 2022, 121, 012102.	1.5	0
10	Ultrathin holey reduced graphene oxide/Ni(picolinic acid)2 papers for flexible battery-supercapacitor hybrid devices. Chemical Engineering Journal, 2021, 408, 127302.	6.6	17
11	Synthesis, luminescent properties and crystal stabilization of GdAG:Mn2+/Ce3+ via Y3+ doping for warm w-LED application. Optical Materials, 2021, 111, 110566.	1.7	7
12	Corncob cellulose-derived hierarchical porous carbon for high performance supercapacitors. Journal of Power Sources, 2021, 484, 229221.	4.0	48
13	High-performance Bi2O3-NC anodes through constructing carbon shells and oxygen vacancies for flexible battery-supercapacitor hybrid devices. Nanoscale Advances, 2021, 3, 593-603.	2.2	8
14	One-step in-situ laser irradiation for unique flocculent carbon network-twined C/Si/SiC composite structure. Ceramics International, 2021, 47, 7101-7105.	2.3	1
15	A novel phosphor of Cu ⁺ -doped PbBrOH: preparation, luminescence mechanism, and outstanding properties. Journal of Materials Chemistry C, 2021, 9, 9178-9187.	2.7	8
16	Postpassivation of Cs _{0.05} (FA _{0.83} MA _{0.17}) _{0.95} Pb(I _{0.83} Br _{0. Perovskite Films with Tris(pentafluorophenyl)borane. ACS Applied Materials & Interfaces, 2021, 13, 2472-2482.}	17) <syb>3</syb>
17	Sustainable fabrication of ultralong Pb(OH)Br nanowires and their conversion to luminescent CH ₃ NH ₃ PbBr ₃ nanowires. Green Chemistry, 2021, 23, 7956-7962.	4.6	3

18Laurionite Competes with 2D Ruddlesdenâ€"Popper Perovskites During the Saturation Recrystallization
Process. ACS Applied Materials & amp; Interfaces, 2021, 13, 6505-6514.4.0

#	Article	IF	CITATIONS
19	Enhanced photocurrent of perovskite solar cells by dual-sensitized β-NaYF4:Nd3+/Yb3+/Er3+ up-conversion nanoparticles. Chemical Physics Letters, 2021, 763, 138253.	1.2	23
20	Plasmonic Au Nanooctahedrons Enhance Light Harvesting and Photocarrier Extraction in Perovskite Solar Cell. ACS Applied Energy Materials, 2021, 4, 3201-3209.	2.5	25
21	Tuning Jahn–Teller distortion and electron localization of LaMnO ₃ epitaxial films via substrate temperature. Journal Physics D: Applied Physics, 2021, 54, 235302.	1.3	11
22	A highly selective and recyclable sensor for the electroanalysis of phosphothioate pesticides using silver-doped ZnO nanorods arrays. Analytica Chimica Acta, 2021, 1152, 338285.	2.6	17
23	Bamboo-like N/S-codoped carbon nanotube aerogels for high-power and high-energy supercapacitors. Journal of Alloys and Compounds, 2021, 861, 157946.	2.8	20
24	Ultrasmall CsPbBr ₃ Quantum Dots with Bright and Wide Blue Emissions. Physica Status Solidi - Rapid Research Letters, 2021, 15, 2100134.	1.2	14
25	Thermal evaporated Cul film thickness-dependent performance of perovskite solar cells. Vacuum, 2021, 187, 110076.	1.6	21
26	In-situ fluorinated 2D/3D invert perovskite film solar cell with enhanced ambient stability. Solar Energy, 2021, 221, 583-590.	2.9	7
27	Large-area CsPbBr3 perovskite films grown with effective one-step RF-magnetron sputtering. Journal of Applied Physics, 2021, 129, .	1.1	9
28	Enhanced upconversion red light emission of TiO ₂ :Yb,Er thin film via Mn doping. Optics Express, 2021, 29, 23159.	1.7	5
29	Heterostructural perovskite solar cell constructed with Li-doped p-MAPbI3/n-TiO2 PN junction. Solar Energy, 2021, 226, 446-454.	2.9	7
30	Enhancing the bulk photovoltaic effect by tuning domain walls in epitaxial BiFeO ₃ films. Nanotechnology, 2021, 32, 495402.	1.3	5
31	Electrochemically constructing V-doped BiFeO3 nanoflake network anodes for flexible asymmetric micro-supercapacitors. Electrochimica Acta, 2021, 393, 139079.	2.6	13
32	Guanidinium cation passivated Pb-Cu alloyed perovskite for efficient low-toxicity solar cells. Applied Surface Science, 2021, 567, 150778.	3.1	6
33	Lead-free Cs2SnX6 (XÂ=ÂCl, Br, I) nanocrystals in mesoporous SiO2 with more stable emission from VIS to NIR light. Chemical Physics Letters, 2021, 782, 139023.	1.2	4
34	Ligand exchange of SnO2 effectively improving the efficiency of flexible perovskite solar cells. Journal of Alloys and Compounds, 2021, 883, 160827.	2.8	14
35	Enhanced photoluminescence of CsPbBr _{3-x} 1 _x nanocrystals via plasmonic Au nanoarrays. Optics Express, 2021, 29, 36988.	1.7	9
36	Epitaxial Growth of Quasi-intrinsic CsPbBr ₃ Film on a SrTiO ₃ Substrate by Pulsed Laser Deposition. ACS Applied Electronic Materials, 2021, 3, 5592-5600.	2.0	7

#	Article	IF	CITATIONS
37	Modifying Jahn-Teller distortion by epitaxial stress in LaMnO3 films for tunning electron localization. Journal of Physics Condensed Matter, 2021, , .	0.7	1
38	High-voltage aqueous asymmetric pseudocapacitors based on methyl blue-doped polyaniline hydrogels and the derived N/S-codoped carbon aerogels. Chemical Engineering Journal, 2020, 383, 123153.	6.6	35
39	Photoluminescence enhancement of perovskite CsPbBr3 quantum dots by plasmonic Au nanorods. Chemical Physics, 2020, 530, 110627.	0.9	19
40	Multifunctional microporous activated carbon nanotubes anchored on graphite fibers for high-strength and high-rate flexible all-solid-state supercapacitors. Applied Surface Science, 2020, 502, 144423.	3.1	15
41	Colorimetric determination of the activity of alkaline phosphatase by exploiting the oxidase-like activity of palladium cube@CeO2 core-shell nanoparticles. Mikrochimica Acta, 2020, 187, 115.	2.5	25
42	Study on the Mn-doped CsPbCl3 perovskite nanocrystals with controllable dual-color emission via energy transfer. Journal of Alloys and Compounds, 2020, 821, 153568.	2.8	27
43	Single Crystal Perovskite Solar Cells: Development and Perspectives. Advanced Functional Materials, 2020, 30, 1905021.	7.8	171
44	Laser assisted self-assembly synthesis of porous hollow MoO3-x-doped MoS2 nanospheres sandwiched by graphene for flexible high-areal supercapacitors. Electrochimica Acta, 2020, 332, 135499.	2.6	23
45	Highly Conductive P-Type MAPbI3 Films and Crystals via Sodium Doping. Frontiers in Chemistry, 2020, 8, 754.	1.8	18
46	Polarization-enhanced bulk photovoltaic effect of BiFeO3 epitaxial film under standard solar illumination. Physics Letters, Section A: General, Atomic and Solid State Physics, 2020, 384, 126831.	0.9	11
47	Study on fluorescence properties and stability of Cu2+-Substituted CsPbBr3 perovskite quantum dots. Physica B: Condensed Matter, 2020, 599, 412488.	1.3	15
48	Corncob-Derived Hierarchical Porous Activated Carbon for High-Performance Lithium-Ion Capacitors. Energy & Fuels, 2020, 34, 16885-16892.	2.5	15
49	Progress and perspective on CsPbX3 nanocrystals for light emitting diodes and solar cells. Journal of Applied Physics, 2020, 128, .	1.1	20
50	From energy harvesting to topologically insulating behavior: ABO ₃ -type epitaxial thin films and superlattices. Journal of Materials Chemistry C, 2020, 8, 15575-15596.	2.7	22
51	Improving the performances of CsPbBr3 solar cells fabricated in ambient condition. Journal of Materials Science: Materials in Electronics, 2020, 31, 21154-21167.	1.1	18
52	Aqueous phase fabrication and conversion of Pb(OH)Br into a CH ₃ NH ₃ PbBr ₃ perovskite and its application in resistive memory switching devices. Green Chemistry, 2020, 22, 3608-3614.	4.6	19
53	Oxygen-deficient BiFeO3-NC nanoflake anodes for flexible battery-supercapacitor hybrid devices with high voltage and long-term stability. Chemical Engineering Journal, 2020, 397, 125524.	6.6	37
54	Combustion procedure deposited SnO2 electron transport layers for high efficient perovskite solar cells. Journal of Alloys and Compounds, 2020, 844, 156032.	2.8	34

#	Article	IF	CITATIONS
55	Electrospun ZnFe2O4/carbon nanofibers as high-rate supercapacitor electrodes. Journal of Power Sources, 2020, 469, 228416.	4.0	38
56	Doping Nitrogen into Q-Graphene by Plasma Treatment toward Peroxidase Mimics with Enhanced Catalysis. Analytical Chemistry, 2020, 92, 5152-5157.	3.2	37
57	Quantum size effect and surface defect passivation in size-controlled CsPbBr3 quantum dots. Journal of Alloys and Compounds, 2020, 831, 154834.	2.8	21
58	Ultrastable Laurionite Spontaneously Encapsulates Reduced-dimensional Lead Halide Perovskites. Nano Letters, 2020, 20, 2316-2325.	4.5	20
59	Efficient Laserâ€Induced Construction of Oxygenâ€Vacancy Abundant Nanoâ€ZnCo ₂ O ₄ /Porous Reduced Graphene Oxide Hybrids toward Exceptional Capacitive Lithium Storage. Small, 2020, 16, e2001526.	5.2	48
60	Good triethylamine sensing properties of Au@MoS2 nanostructures directly grown on ceramic tubes. Materials Chemistry and Physics, 2020, 245, 122683.	2.0	17
61	Highly conductive n-type CH ₃ NH ₃ PbI ₃ single crystals doped with bismuth donors. Journal of Materials Chemistry C, 2020, 8, 3694-3704.	2.7	27
62	Mono-dispersed Ag/Graphene nanocomposite as lubricant additive to reduce friction and wear. Tribology International, 2020, 146, 106228.	3.0	89
63	Study on synthesis and luminescent properties of Mn4+ doped (Gd,Y)3Al5O12 phosphor. Optical Materials, 2020, 102, 109815.	1.7	10
64	Zwitterion-Stabilizing Scalable Bladed α-Phase Cs _{0.1} FA _{0.9} PbI ₃ Films for Efficient Inverted Planar Perovskite Solar Cells. ACS Sustainable Chemistry and Engineering, 2020, 8, 7020-7030.	3.2	27
65	Study on organic-inorganic hybrid perovskite nanocrystals with regular morphologies and their effect on photoluminescence properties. Optics Express, 2020, 28, 10714.	1.7	7
66	Study on MA(Pb,Cu)Br3 Provskite Nanocrystal with Both Controlled Color Emission and Improved Stability. ES Materials & Manufacturing, 2020, , .	1.1	1
67	Enhanced triethylamine sensing performance of α-Fe2O3 nanoparticle/ZnO nanorod heterostructures. Sensors and Actuators B: Chemical, 2019, 298, 126917.	4.0	74
68	Bismuth Telluride Interlayer for Allâ€inorganic Perovskite Solar Cells with Enhanced Efficiency and Stability. Solar Rrl, 2019, 3, 1900233.	3.1	27
69	Copper submicrospheres induced by pulsed laser-irradiation with enhanced tribology properties. New Journal of Chemistry, 2019, 43, 13526-13535.	1.4	4
70	Ligand induced anomalous emission shift of size-controlled CsPbBr3 nanocrystals. Applied Physics Letters, 2019, 115, .	1.5	16
71	Fe ₃ O ₄ Nanozymes with Aptamer-Tuned Catalysis for Selective Colorimetric Analysis of ATP in Blood. Analytical Chemistry, 2019, 91, 14737-14742.	3.2	105
72	Highly transparent and conductive Î ³ -Cul films grown by simply dipping copper films into iodine solution. Physica B: Condensed Matter, 2019, 573, 45-48.	1.3	23

#	Article	IF	CITATIONS
73	Gold nanoclusters-based dual-channel assay for colorimetric and turn-on fluorescent sensing of alkaline phosphatase. Sensors and Actuators B: Chemical, 2019, 301, 127080.	4.0	60
74	Enhanced performance of TiO2-based planar perovskite solar cells by In2O3 interfacial modification layer. Organic Electronics, 2019, 75, 105426.	1.4	11
75	Enhanced Triethylamine Sensing Properties by Designing an α-Fe ₂ O ₃ /α-MoO ₃ Nanostructure Directly Grown on Ceramic Tubes. ACS Applied Nano Materials, 2019, 2, 6715-6725.	2.4	36
76	Threeâ€Dimensional Mesoporous Strawâ€like Co 3 O 4 Anode with Enhanced Electrochemical Performance for Lithiumâ€lon Batteries. ChemistrySelect, 2019, 4, 6879-6885.	0.7	7
77	Facile fabrication of porous NiMoO4@C nanowire as high performance anode material for lithium ion batteries. Ceramics International, 2019, 45, 18462-18470.	2.3	24
78	Corncob-derived hierarchical porous carbons constructed by re-activation for high-rate lithium-ion capacitors. New Journal of Chemistry, 2019, 43, 10103-10108.	1.4	10
79	Laser induced oxygen-deficient TiO2/graphene hybrid for high-performance supercapacitor. Journal of Power Sources, 2019, 431, 220-225.	4.0	54
80	Hierarchical Porous Activated Carbon Obtained by a Novel Heatingâ€Rateâ€Induced Method for Lithiumâ€Ion Capacitor. ChemistrySelect, 2019, 4, 5300-5307.	0.7	7
81	Sealing the domain boundaries and defects passivation by Poly(acrylic acid) for scalable blading of efficient perovskite solar cells. Journal of Power Sources, 2019, 426, 188-196.	4.0	29
82	Rod-like porous CoMoO4@C as excellent anode for high performance lithium ion battery. Journal of Alloys and Compounds, 2019, 790, 891-899.	2.8	35
83	Perovskite films grown with green mixed anti-solvent for highly efficient solar cells with enhanced stability. Solar Energy, 2019, 181, 285-292.	2.9	41
84	Controllable ZnFe2O4/reduced graphene oxide hybrid for high-performance supercapacitor electrode. Electrochimica Acta, 2018, 268, 20-26.	2.6	65
85	Green laser irradiation-stimulated fullerene-like MoS2 nanospheres for tribological applications. Tribology International, 2018, 122, 119-124.	3.0	23
86	Laser irradiation-induced laminated graphene/MoS ₂ composites with synergistically improved tribological properties. Nanotechnology, 2018, 29, 265704.	1.3	26
87	Enhanced triethylamine sensing properties by fabricating Au@SnO2/α-Fe2O3 core-shell nanoneedles directly on alumina tubes. Sensors and Actuators B: Chemical, 2018, 262, 70-78.	4.0	96
88	Enhanced triethylamine sensing properties by designing Au@SnO 2 /ZnO nanosheets directly on alumina tubes. Surfaces and Interfaces, 2018, 10, 85-92.	1.5	30
89	Oxygenâ€Vacancy Abundant Ultrafine Co ₃ O ₄ /Graphene Composites for Highâ€Rate Supercapacitor Electrodes. Advanced Science, 2018, 5, 1700659.	5.6	392
90	Room-temperature, high selectivity and low-ppm-level triethylamine sensor assembled with Au decahedrons-decorated porous α-Fe2O3 nanorods directly grown on flat substrate. Sensors and Actuators B: Chemical, 2018, 268, 170-181.	4.0	72

#	Article	IF	CITATIONS
91	Tribology Properties: Laser Irradiationâ€Induced SiC@Graphene Subâ€Microspheres: A Bioinspired Core–Shell Structure for Enhanced Tribology Properties (Adv. Mater. Interfaces 5/2018). Advanced Materials Interfaces, 2018, 5, 1870021.	1.9	2
92	ZnFe2O4 nanoparticles-cotton derived hierarchical porous active carbon fibers for high rate-capability supercapacitor electrodes. Carbon, 2018, 134, 15-21.	5.4	76
93	Excess iodine as the interface recombination center limiting the open-circuit voltage of Cul-based perovskite planar solar cell. Journal of Materials Science: Materials in Electronics, 2018, 29, 8838-8846.	1.1	9
94	Laser Irradiationâ€Induced SiC@Graphene Subâ€Microspheres: A Bioinspired Core–Shell Structure for Enhanced Tribology Properties. Advanced Materials Interfaces, 2018, 5, 1700839.	1.9	10
95	Low-temperature in-situ growth of SnO2 nanosheets and its high triethylamine sensing response by constructing Au-loaded ZnO/SnO2 heterostructure. Journal of Alloys and Compounds, 2018, 737, 603-612.	2.8	72
96	Highly transparent 3D NiO-Ni/Ag-nanowires/FTO micro-supercapacitor electrodes for fully transparent electronic deviceÂpurpose. Electrochimica Acta, 2018, 260, 281-289.	2.6	23
97	Monolithic perovskite/Si tandem solar cells exceeding 22% efficiency via optimizing top cell absorber. Nano Energy, 2018, 53, 798-807.	8.2	83
98	Reversible Band Gap Narrowing of Snâ€Based Hybrid Perovskite Single Crystal with Excellent Phase Stability. Angewandte Chemie, 2018, 130, 15084-15088.	1.6	17
99	Preparation of defective ZnFe2O4/graphene composites and their charge storage properties. Electrochemistry Communications, 2018, 92, 19-23.	2.3	32
100	A novel hetero-structure sensor based on Au/Mg-doped TiO2/SnO2 nanosheets directly grown on Al2O3 ceramic tubes. Sensors and Actuators B: Chemical, 2018, 273, 328-335.	4.0	35
101	Ultrafast synthesis of SiC@graphene nanocomposites by one-step laser induced fragmentation and decomposition. Ceramics International, 2018, 44, 19028-19032.	2.3	8
102	Surface-crumpled graphene hydrogels with macro- and microporous structures for ultrahigh-volumetric energy storage. Journal of Power Sources, 2018, 399, 115-124.	4.0	39
103	Zinc as a New Dopant for NiO _{<i>x</i>} -Based Planar Perovskite Solar Cells with Stable Efficiency near 20%. ACS Applied Energy Materials, 2018, 1, 3947-3954.	2.5	87
104	Flexible and Biocompatibility Power Source for Electronics: A Cellulose Paper Based Holeâ€Transportâ€Materialsâ€Free Perovskite Solar Cell. Solar Rrl, 2018, 2, 1800175.	3.1	37
105	Improving the triethylamine sensing performance based on debye length: A case study on α-Fe2O3@NiO(CuO) core-shell nanorods sensor working at near room-temperature. Sensors and Actuators B: Chemical, 2017, 245, 375-385.	4.0	75
106	Different morphologies of ZnO and their triethylamine sensing properties. Journal of Alloys and Compounds, 2017, 706, 461-469.	2.8	64
107	The air and thermal stabilities of lead-free perovskite variant Cs 2 SnI 6 powder. Materials Letters, 2017, 199, 50-52.	1.3	59
108	Welded-Ag-nanowires/FTO conducting film with high transmittance and its application in transparent supercapacitors. IOP Conference Series: Materials Science and Engineering, 2017, 182, 012022.	0.3	0

#	Article	IF	CITATIONS
109	SnO 2 nanotube arrays grown via an in situ template-etching strategy for effective and stable perovskite solar cells. Chemical Engineering Journal, 2017, 325, 378-385.	6.6	52
110	Construction of hollow Co ₃ O ₄ cubes as a high-performance anode for lithium ion batteries. New Journal of Chemistry, 2017, 41, 7960-7965.	1.4	28
111	Highly sensitive gold-decorated zinc oxide nanorods sensor for triethylamine working at near room temperature. Journal of Colloid and Interface Science, 2017, 499, 67-75.	5.0	57
112	High-sensitivity, high-selectivity, and fast-recovery-speed triethylamine sensor based on ZnO micropyramids prepared by molten salt growth method. Journal of Alloys and Compounds, 2017, 695, 2930-2936.	2.8	65
113	Two-dimensional porous Co ₃ O ₄ nanosheets for high-performance lithium ion batteries. New Journal of Chemistry, 2017, 41, 15283-15288.	1.4	25
114	Enhanced triethylamine sensing properties by designing Au@SnO2/MoS2 nanostructure directly on alumina tubes. Sensors and Actuators B: Chemical, 2017, 253, 97-107.	4.0	97
115	Enhanced physical properties of pulsed laser deposited NiO films via annealing and lithium doping for improving perovskite solar cell efficiency. Journal of Materials Chemistry C, 2017, 5, 7084-7094.	2.7	134
116	From unstable CsSnI3 to air-stable Cs2SnI6: A lead-free perovskite solar cell light absorber with bandgap of 1.48 eV and high absorption coefficient. Solar Energy Materials and Solar Cells, 2017, 159, 227-234.	3.0	388
117	The Influence of Physical Properties of ZnO Films on the Efficiency of Planar ZnO/Perovskite/P3HT Solar Cell. Journal of the American Ceramic Society, 2017, 100, 176-184.	1.9	22
118	Hierarchical Co ₃ O ₄ Nanowires as Binder Free Electrodes for Reversible Lithium Storage. Chinese Journal of Chemistry, 2016, 34, 631-636.	2.6	6
119	Oxygen influencing the photocarriers lifetime of CH3NH3PbI3â^'xClx film grown by two-step interdiffusion method and its photovoltaic performance. Applied Physics Letters, 2016, 108, .	1.5	26
120	Growth temperature-dependent performance of planar CH ₃ NH ₃ PbI ₃ solar cells fabricated by a two-step subliming vapor method below 120 °C. RSC Advances, 2016, 6, 47459-47467.	1.7	7
121	High-Quality Perovskite Films Grown with a Fast Solvent-Assisted Molecule Inserting Strategy for Highly Efficient and Stable Solar Cells. ACS Applied Materials & Interfaces, 2016, 8, 22238-22245.	4.0	19
122	Leadâ€free mesoscopic Cs ₂ SnI ₆ perovskite solar cells using different nanostructured ZnO nanorods as electron transport layers. Physica Status Solidi - Rapid Research Letters, 2016, 10, 587-591.	1.2	138
123	Smooth and solid WS ₂ submicrospheres grown by a new laser fragmentation and reshaping process with enhanced tribological properties. Chemical Communications, 2016, 52, 10147-10150.	2.2	33
124	3D hierarchical MnO ₂ nanorod/welded Ag-nanowire-network composites for high-performance supercapacitor electrodes. Chemical Communications, 2016, 52, 7998-8001.	2.2	56
125	Superior triethylamine-sensing properties based on TiO2/SnO2 n–n heterojunction nanosheets directly grown on ceramic tubes. Sensors and Actuators B: Chemical, 2016, 228, 634-642.	4.0	134
126	Au nanoparticle-functionalized 3D SnO2 microstructures for high performance gas sensor. Sensors and Actuators B: Chemical, 2016, 226, 266-272.	4.0	124

#	Article	IF	CITATIONS
127	Low-working-temperature, fast-response-speed NO2 sensor with nanoporous-SnO2/polyaniline double-layered film. Sensors and Actuators B: Chemical, 2016, 224, 654-660.	4.0	72
128	Near room-temperature triethylamine sensor constructed with CuO/ZnO P-N heterostructural nanorods directly on flat electrode. Sensors and Actuators B: Chemical, 2016, 225, 16-23.	4.0	143
129	Effect of deposition temperature on transparent conductive properties of γ-Cul film prepared by vacuum thermal evaporation. Physica Status Solidi (A) Applications and Materials Science, 2015, 212, 1466-1470.	0.8	68
130	Indium-free Cu/fluorine doped ZnO composite transparent conductive electrodes with stretchable and flexible performance on poly(ethylene terephthalate) substrate. Applied Surface Science, 2015, 332, 549-556.	3.1	8
131	Phosphorus Concentration Dependent Microstructure and Optical Property of ZnO Nanowires Grown by High-Pressure Pulsed Laser Deposition. Journal of Physical Chemistry C, 2015, 119, 4371-4378.	1.5	18
132	Morphology-modulation of SnO2 Hierarchical Architectures by Zn Doping for Glycol Gas Sensing and Photocatalytic Applications. Scientific Reports, 2015, 5, 7874.	1.6	112
133	Fully indium-free flexible Ag nanowires/ZnO:F composite transparent conductive electrodes with high haze. Journal of Materials Chemistry A, 2015, 3, 5375-5384.	5.2	125
134	3D hierarchical Co ₃ O ₄ microspheres with enhanced lithium-ion battery performance. RSC Advances, 2015, 5, 61631-61638.	1.7	25
135	High triethylamine-sensing properties of NiO/SnO2 hollow sphere P–N heterojunction sensors. Sensors and Actuators B: Chemical, 2015, 215, 39-44.	4.0	203
136	Hierarchical Co@C Nanoflowers: Synthesis and Electrochemical Properties as an Advanced Negative Material for Alkaline Secondary Batteries. ACS Applied Materials & Interfaces, 2015, 7, 23978-23983.	4.0	19
137	Morphology Evolution of ZnO Submicroparticles Induced by Laser Irradiation and Their Enhanced Tribology Properties by Compositing with Al ₂ O ₃ Nanoparticles. Advanced Engineering Materials, 2015, 17, 341-348.	1.6	14
138	Sodiumâ€Doped ZnO Nanowires Grown by Highâ€pressure <scp>PLD</scp> and their Acceptorâ€Related Optical Properties. Journal of the American Ceramic Society, 2014, 97, 2177-2184.	1.9	26
139	Highly sensitive and selective triethylamine-sensing properties of nanosheets directly grown on ceramic tube by forming NiO/ZnO PN heterojunction. Sensors and Actuators B: Chemical, 2014, 200, 288-296.	4.0	209
140	A novel TiO2 nanorod/nanoparticle composite architecture to improve the performance of dye-sensitized solar cells. Ceramics International, 2014, 40, 2337-2342.	2.3	26
141	ZnO photoanodes with different morphologies grown by electrochemical deposition and their dye-sensitized solar cell properties. Ceramics International, 2014, 40, 7965-7970.	2.3	47
142	TiO ₂ @C composite nanospheres with an optimized homogeneous structure for lithium-ion batteries. New Journal of Chemistry, 2014, 38, 3722-3728.	1.4	14
143	Submicron-Lubricant Based on Crystallized Fe ₃ O ₄ Spheres for Enhanced Tribology Performance. Chemistry of Materials, 2014, 26, 5113-5119.	3.2	59
144	Direct hydrothermal growth of ZnO nanosheets on electrode for ethanol sensing. Sensors and Actuators B: Chemical, 2014, 201, 444-451.	4.0	96

#	Article	IF	CITATIONS
145	The influence of annealing temperature on the interface and photovoltaic properties of CdS/CdSe quantum dots sensitized ZnO nanorods solar cells. Journal of Colloid and Interface Science, 2014, 430, 200-206.	5.0	13
146	High-performance gas sensor based on ZnO nanowires functionalized by Au nanoparticles. Sensors and Actuators B: Chemical, 2014, 199, 339-345.	4.0	274
147	CdS and CdS/CdSe sensitized ZnO nanorod array solar cells prepared by a solution ions exchange process. Materials Research Bulletin, 2013, 48, 4261-4266.	2.7	15
148	Reactive-Template Fabrication of Porous SnO ₂ Nanotubes and Their Remarkable Gas-Sensing Performance. ACS Applied Materials & Interfaces, 2013, 5, 7893-7898.	4.0	169
149	Zn1â^'x Mg x O (0≤â‰0.05) nanowalls grown on catalyst-free sapphire substrates by high-pressure PLD and their photoluminescence properties. Applied Physics A: Materials Science and Processing, 2013, 111, 1119-1124.	1.1	1
150	Three-dimensional SnO2 microstructures assembled by porous nanosheets and their superior performance for gas sensing. Powder Technology, 2013, 250, 40-45.	2.1	43
151	Microwave-assisted hydrothermal synthesis and gas sensitivity of nanostructured SnO2. Particuology, 2013, 11, 242-248.	2.0	18
152	NO2 gas sensing with SnO2–ZnO/PANI composite thick film fabricated from porous nanosolid. Sensors and Actuators B: Chemical, 2013, 176, 166-173.	4.0	97
153	One-pot fabrication of uniform polypyrrole/Au nanocomposites and investigation for gas sensing. Sensors and Actuators B: Chemical, 2013, 186, 695-700.	4.0	72
154	Largeâ€Scale Fabrication of Threeâ€Dimensional Surface Patterns Using Templateâ€Defined Electrochemical Deposition. Advanced Functional Materials, 2013, 23, 720-730.	7.8	67
155	Reactive Template Synthesis of Polypyrrole Nanotubes for Fabricating Metal/Conducting Polymer Nanocomposites. Macromolecular Rapid Communications, 2013, 34, 528-532.	2.0	46
156	Laser-induced reshaping of particles aiming at energy-saving applications. Journal of Materials Chemistry, 2012, 22, 15947.	6.7	39
157	One-pot synthesis of Au-supported ZnO nanoplates with enhanced gas sensor performance. Sensors and Actuators B: Chemical, 2012, 169, 61-66.	4.0	139
158	Fabrication and Characterization of Beaded SiC Quantum Rings with Anomalous Red Spectral Shift. Advanced Materials, 2012, 24, 5598-5603.	11.1	65
159	Aqueous Synthesis of CdTe and HgCdTe Quantum Dots and Their Application in Quantum Dot-Sensitized Solar Cells. Science of Advanced Materials, 2012, 4, 337-341.	0.1	4
160	Synthesis of monodispersed ZnAl2O4 nanoparticles and their tribology properties as lubricant additives. Materials Research Bulletin, 2012, 47, 4305-4310.	2.7	96
161	A new method for surface modification of TiO2/Al2O3 nanocomposites with enhanced anti-friction properties. Materials Chemistry and Physics, 2012, 134, 38-42.	2.0	18
162	Synthesis and catalytic activity of Au-supported porous TiO2 nanospheres for CO oxidation. Powder Technology, 2012, 217, 585-590.	2.1	11

#	Article	IF	CITATIONS
163	Enhanced tribology properties of ZnO/Al2O3 composite nanoparticles as liquid lubricating additives. Journal of Sol-Gel Science and Technology, 2012, 61, 501-508.	1.1	21
164	Template-directed dewetting of a gold membrane to fabricate highly SERS-active substrates. Journal of Materials Chemistry, 2011, 21, 14031.	6.7	28
165	Three kinds of Cu2O/ZnO heterostructure solar cells fabricated with electrochemical deposition and their structure-related photovoltaic properties. CrystEngComm, 2011, 13, 6065.	1.3	70
166	Origin of Blue Emission from Silicon Nanoparticles: Direct Transition and Interface Recombination. Journal of Physical Chemistry C, 2011, 115, 21056-21062.	1.5	92
167	Influences of Target and Liquid Media on Morphologies and Optical Properties of <scp>ZnO</scp> Nanoparticles Prepared by Laser Ablation in Solution. Journal of the American Ceramic Society, 2011, 94, 4305-4309.	1.9	18
168	Microwave hydrothermal synthesis of nanoporous cobalt oxides and their gas sensing properties. Materials Research Bulletin, 2011, 46, 1097-1101.	2.7	35
169	Friction and wear properties of ZrO2/SiO2 composite nanoparticles. Journal of Nanoparticle Research, 2011, 13, 2129-2137.	0.8	96
170	The tribology properties of alumina/silica composite nanoparticles as lubricant additives. Applied Surface Science, 2011, 257, 5720-5725.	3.1	199
171	Selfâ€organized growth of ZnOâ€based nano―and microstructures. Physica Status Solidi (B): Basic Research, 2010, 247, 1265-1281.	0.7	41
172	Whispering gallery modes in zinc oxide micro―and nanowires. Physica Status Solidi (B): Basic Research, 2010, 247, 1282-1293.	0.7	77
173	Electrochemical Deposition of ZnO Nanowire Arrays: Organization, Doping, and Properties. Science of Advanced Materials, 2010, 2, 336-358.	0.1	62
174	Optical characterization of zinc oxide microlasers and microwire core-shell heterostructures. Journal of Vacuum Science & Technology B, 2009, 27, 1780.	1.3	6
175	Morphology Evolution and CL Property of Ni-Doped Zinc Oxide Nanostructures with Room-Temperature Ferromagnetism. Journal of Physical Chemistry C, 2009, 113, 4381-4385.	1.5	74
176	Stable p-type ZnO:P nanowire/n-type ZnO:Ga film junctions, reproducibly grown by two-step pulsed laser deposition. Journal of Vacuum Science & Technology B, 2009, 27, 1693-1697.	1.3	18
177	From ZnO Nanorods to Nanoplates:  Chemical Bath Deposition Growth and Surface-Related Emissions. Journal of Physical Chemistry C, 2008, 112, 680-685.	1.5	225
178	Whispering gallery mode lasing in zinc oxide microwires. Applied Physics Letters, 2008, 92, 241102.	1.5	192
179	Temperature-Dependent Emission Shifts of Peanutlike ZnO Microrods Synthesized by a Hydrothermal Method. Crystal Growth and Design, 2007, 7, 1686-1689.	1.4	23
180	Different ZnO Nanostructures Fabricated by a Seed-Layer Assisted Electrochemical Route and Their Photoluminescence and Field Emission Properties. Journal of Physical Chemistry C, 2007, 111, 2470-2476.	1.5	138

#	Article	IF	CITATIONS
181	Microstructure Control of Zn/ZnO Core/Shell Nanoparticles and Their Temperature-Dependent Blue Emissions. Journal of Physical Chemistry B, 2007, 111, 14311-14317.	1.2	143
182	Transferable Ordered Ni Hollow Sphere Arrays Induced by Electrodeposition on Colloidal Monolayer. Journal of Physical Chemistry B, 2006, 110, 7184-7188.	1.2	64
183	Two-dimensional hierarchical porous silica film and its tunable superhydrophobicity. Nanotechnology, 2006, 17, 238-243.	1.3	144
184	Morphology evolution and photoluminescence properties of ZnO films electrochemically deposited on conductive glass substrates. Journal of Applied Physics, 2006, 99, 073516.	1.1	114
185	Morphology-controlled 2D ordered arrays by heating-induced deformation of 2D colloidal monolayer. Journal of Materials Chemistry, 2006, 16, 609-612.	6.7	43
186	Temperature-dependent shifts of three emission bands for ZnO nanoneedle arrays. Applied Physics Letters, 2006, 88, 161101.	1.5	296
187	Growth of ZnO Nanoneedle Arrays with Strong Ultraviolet Emissions by an Electrochemical Deposition Method. Crystal Growth and Design, 2006, 6, 1091-1095.	1.4	68
188	Fabrication of the periodic nanopillar arrays by heat-induced deformation of 2D polymer colloidal monolayer. Polymer, 2005, 46, 12033-12036.	1.8	28
189	2D nanoparticle arrays by partial dissolution of ordered pore films. Materials Letters, 2005, 59, 276-279.	1.3	17
190	Superhydrophobicity of 2D ZnO ordered pore arrays formed by solution-dipping template method. Journal of Colloid and Interface Science, 2005, 287, 634-639.	5.0	172
191	Two-dimensional ordered polymer hollow sphere and convex structure arrays based on monolayer pore films. Journal of Materials Research, 2005, 20, 338-343.	1.2	21
192	Electrodeposition-Induced Highly Oriented Zinc Oxide Ordered Pore Arrays and Their Ultraviolet Emissions. Electrochemical and Solid-State Letters, 2005, 8, G237.	2.2	29
193	Ultraviolet-light-emitting ZnO nanosheets prepared by a chemical bath deposition method. Nanotechnology, 2005, 16, 1734-1738.	1.3	124
194	A template-free electrochemical deposition route to ZnO nanoneedle arrays and their optical and field emission properties. Nanotechnology, 2005, 16, 2567-2574.	1.3	114
195	Fabrication of large-scale zinc oxide ordered pore arrays with controllable morphology. Chemical Communications, 2004, , 1604.	2.2	55